

Measurement of Two-Particle Correlations of Hadrons in e^+e^- Collisions at Belle

Y.-C. Chen,^{59,*} Y.-J. Lee,^{59,*} P. Chang,⁵⁹ I. Adachi,^{19,16} H. Aihara,⁸⁴ S. Al Said,^{78,39} D. M. Asner,³ T. Aushev,²¹ R. Ayad,⁷⁸ V. Babu,⁸ P. Behera,²⁷ K. Belous,³⁰ J. Bennett,⁵² M. Bessner,¹⁸ T. Bilka,⁵ D. Bodrov,^{21,44} J. Borah,²⁵ M. Bračko,^{49,36} P. Branchini,³² T. E. Browder,¹⁸ A. Budano,³² M. Campajola,^{31,56} D. Červenkov,⁵ M.-C. Chang,¹² V. Chekelian,⁵⁰ B. G. Cheon,¹⁷ K. Chilikin,⁴⁴ H. E. Cho,¹⁷ K. Cho,⁴¹ S.-J. Cho,⁸⁸ S.-K. Choi,⁶ Y. Choi,⁷⁶ D. Cinabro,⁸⁷ S. Das,⁴⁸ G. De Nardo,^{31,56} G. De Pietro,³² R. Dhamija,²⁶ F. Di Capua,^{31,56} J. Dingfelder,² T. V. Dong,¹⁰ D. Dossett,⁵¹ D. Epifanov,^{4,62} T. Ferber,⁸ B. G. Fulsom,⁶⁴ R. Garg,⁶⁵ V. Gaur,⁸⁶ A. Giri,²⁶ P. Goldenzweig,³⁷ T. Gu,⁶⁶ K. Gudkova,^{4,62} C. Hadjivasiliou,⁶⁴ O. Hartbrich,¹⁸ K. Hayasaka,⁶¹ H. Hayashii,⁵⁷ W.-S. Hou,⁵⁹ C.-L. Hsu,⁷⁷ T. Iijima,^{55,54} K. Inami,⁵⁴ A. Ishikawa,^{19,16} R. Itoh,^{19,16} M. Iwasaki,⁶³ Y. Iwasaki,¹⁹ W. W. Jacobs,²⁸ S. Jia,¹³ Y. Jin,⁸⁴ A. B. Kaliyar,⁷⁹ C. H. Kim,¹⁷ D. Y. Kim,⁷⁵ K.-H. Kim,⁸⁸ Y.-K. Kim,⁸⁸ P. Kodyš,⁵ T. Konno,⁴⁰ A. Korobov,^{4,62} S. Korpar,^{49,36} E. Kovalenko,^{4,62} P. Križan,^{45,36} R. Kroeger,⁵² P. Krokovny,^{4,62} M. Kumar,⁴⁸ R. Kumar,⁶⁷ K. Kumara,⁸⁷ A. Kuzmin,^{4,62,44} Y.-J. Kwon,⁸⁸ Y.-T. Lai,³⁸ T. Lam,⁸⁶ J. S. Lange,¹⁴ M. Lorenza,^{32,71} S. C. Lee,⁴³ J. Li,⁴³ Y. Li,¹³ Y. B. Li,¹³ L. Li Gioi,⁵⁰ J. Libby,²⁷ K. Lieret,⁴⁶ C.-W. Lin,⁵⁹ D. Liventsev,^{87,19} A. Martini,⁸⁹ M. Masuda,^{83,68} T. Matsuda,⁵³ D. Matvienko,^{4,62,44} F. Meier,⁹ M. Merola,^{31,56} F. Metzner,³⁷ K. Miyabayashi,⁵⁷ G. B. Mohanty,⁷⁹ T. J. Moon,⁷³ R. Mussa,³³ M. Nakao,^{19,16} A. Natochii,¹⁸ L. Nayak,²⁶ N. K. Nisar,³ S. Nishida,^{19,16} K. Nishimura,¹⁸ S. Ogawa,⁸¹ H. Ono,^{60,61} G. Pakhlova,^{21,44} T. Pang,⁶⁶ S. Pardi,³¹ S.-H. Park,¹⁹ S. Patra,²⁴ S. Paul,^{80,50} T. K. Pedlar,⁴⁷ L. E. Piilonen,⁸⁶ T. Podobnik,^{45,36} E. Prencipe,²² M. T. Prim,² N. Rout,²⁷ G. Russo,⁵⁶ D. Sahoo,³⁴ S. Sandilya,²⁶ A. Sangal,⁷ L. Santelj,^{45,36} T. Sanuki,⁸² V. Savinov,⁶⁶ G. Schnell,^{1,23} C. Schwanda,²⁹ R. Seidl,⁷⁰ Y. Seino,⁶¹ M. E. Sevier,⁵¹ M. Shapkin,³⁰ J.-G. Shiu,⁵⁹ J. B. Singh,^{65,†} A. Sokolov,³⁰ E. Solovieva,⁴⁴ M. Starič,³⁶ Z. S. Stottler,⁸⁶ M. Sumihama,¹⁵ K. Sumisawa,^{19,16} W. Sutcliffe,² M. Takizawa,^{74,20,69} U. Tamponi,³³ K. Tanida,³⁵ F. Tenchini,⁸ M. Uchida,⁸⁵ T. Uglov,^{44,21} Y. Unno,¹⁷ K. Uno,⁶¹ S. Uno,^{19,16} R. Van Tonder,² G. Varner,¹⁸ A. Vinokurova,^{4,62} A. Vossen,⁹ E. Waheed,¹⁹ C. H. Wang,⁵⁸ D. Wang,¹¹ E. Wang,⁶⁶ X. L. Wang,¹³ S. Watanuki,⁸⁸ E. Won,⁴² W. Yan,⁷² S. B. Yang,⁴² H. Ye,⁸ J. Yelton,¹¹ Y. Zhai,³⁴ Z. P. Zhang,⁷² V. Zhilich,^{4,62} and V. Zhukova⁴⁴

(The Belle Collaboration)

¹*Department of Physics, University of the Basque Country UPV/EHU, 48080 Bilbao*

²*University of Bonn, 53115 Bonn*

³*Brookhaven National Laboratory, Upton, New York 11973*

⁴*Budker Institute of Nuclear Physics SB RAS, Novosibirsk 630090*

⁵*Faculty of Mathematics and Physics, Charles University, 121 16 Prague*

⁶*Chung-Ang University, Seoul 06974*

⁷*University of Cincinnati, Cincinnati, Ohio 45221*

⁸*Deutsches Elektronen-Synchrotron, 22607 Hamburg*

⁹*Duke University, Durham, North Carolina 27708*

¹⁰*Institute of Theoretical and Applied Research (ITAR), Duy Tan University, Hanoi 100000*

¹¹*University of Florida, Gainesville, Florida 32611*

¹²*Department of Physics, Fu Jen Catholic University, Taipei 24205*

¹³*Key Laboratory of Nuclear Physics and Ion-beam Application (MOE)*

and Institute of Modern Physics, Fudan University, Shanghai 200443

¹⁴*Justus-Liebig-Universität Gießen, 35392 Gießen*

¹⁵*Gifu University, Gifu 501-1193*

¹⁶*SOKENDAI (The Graduate University for Advanced Studies), Hayama 240-0193*

¹⁷*Department of Physics and Institute of Natural Sciences, Hanyang University, Seoul 04763*

¹⁸*University of Hawaii, Honolulu, Hawaii 96822*

¹⁹*High Energy Accelerator Research Organization (KEK), Tsukuba 305-0801*

²⁰*J-PARC Branch, KEK Theory Center, High Energy Accelerator Research Organization (KEK), Tsukuba 305-0801*

²¹*National Research University Higher School of Economics, Moscow 101000*

²²*Forschungszentrum Jülich, 52425 Jülich*

²³*IKERBASQUE, Basque Foundation for Science, 48013 Bilbao*

²⁴*Indian Institute of Science Education and Research Mohali, SAS Nagar, 140306*

²⁵*Indian Institute of Technology Guwahati, Assam 781039*

²⁶*Indian Institute of Technology Hyderabad, Telangana 502285*

²⁷*Indian Institute of Technology Madras, Chennai 600036*

²⁸*Indiana University, Bloomington, Indiana 47408*

- ²⁹Institute of High Energy Physics, Vienna 1050
- ³⁰Institute for High Energy Physics, Protvino 142281
- ³¹INFN - Sezione di Napoli, I-80126 Napoli
- ³²INFN - Sezione di Roma Tre, I-00146 Roma
- ³³INFN - Sezione di Torino, I-10125 Torino
- ³⁴Iowa State University, Ames, Iowa 50011
- ³⁵Advanced Science Research Center, Japan Atomic Energy Agency, Naka 319-1195
- ³⁶J. Stefan Institute, 1000 Ljubljana
- ³⁷Institut für Experimentelle Teilchenphysik, Karlsruhe Institut für Technologie, 76131 Karlsruhe
- ³⁸Kavli Institute for the Physics and Mathematics of the Universe (WPI), University of Tokyo, Kashiwa 277-8583
- ³⁹Department of Physics, Faculty of Science, King Abdulaziz University, Jeddah 21589
- ⁴⁰Kitasato University, Sagamihara 252-0373
- ⁴¹Korea Institute of Science and Technology Information, Daejeon 34141
- ⁴²Korea University, Seoul 02841
- ⁴³Kyungpook National University, Daegu 41566
- ⁴⁴P.N. Lebedev Physical Institute of the Russian Academy of Sciences, Moscow 119991
- ⁴⁵Faculty of Mathematics and Physics, University of Ljubljana, 1000 Ljubljana
- ⁴⁶Ludwig Maximilians University, 80539 Munich
- ⁴⁷Luther College, Decorah, Iowa 52101
- ⁴⁸Malaviya National Institute of Technology Jaipur, Jaipur 302017
- ⁴⁹Faculty of Chemistry and Chemical Engineering, University of Maribor, 2000 Maribor
- ⁵⁰Max-Planck-Institut für Physik, 80805 München
- ⁵¹School of Physics, University of Melbourne, Victoria 3010
- ⁵²University of Mississippi, University, Mississippi 38677
- ⁵³University of Miyazaki, Miyazaki 889-2192
- ⁵⁴Graduate School of Science, Nagoya University, Nagoya 464-8602
- ⁵⁵Kobayashi-Maskawa Institute, Nagoya University, Nagoya 464-8602
- ⁵⁶Università di Napoli Federico II, I-80126 Napoli
- ⁵⁷Nara Women's University, Nara 630-8506
- ⁵⁸National United University, Miao Li 36003
- ⁵⁹Department of Physics, National Taiwan University, Taipei 10617
- ⁶⁰Nippon Dental University, Niigata 951-8580
- ⁶¹Niigata University, Niigata 950-2181
- ⁶²Novosibirsk State University, Novosibirsk 630090
- ⁶³Osaka City University, Osaka 558-8585
- ⁶⁴Pacific Northwest National Laboratory, Richland, Washington 99352
- ⁶⁵Panjab University, Chandigarh 160014
- ⁶⁶University of Pittsburgh, Pittsburgh, Pennsylvania 15260
- ⁶⁷Punjab Agricultural University, Ludhiana 141004
- ⁶⁸Research Center for Nuclear Physics, Osaka University, Osaka 567-0047
- ⁶⁹Meson Science Laboratory, Cluster for Pioneering Research, RIKEN, Saitama 351-0198
- ⁷⁰RIKEN BNL Research Center, Upton, New York 11973
- ⁷¹Dipartimento di Matematica e Fisica, Università di Roma Tre, I-00146 Roma
- ⁷²Department of Modern Physics and State Key Laboratory of Particle Detection and Electronics, University of Science and Technology of China, Hefei 230026
- ⁷³Seoul National University, Seoul 08826
- ⁷⁴Showa Pharmaceutical University, Tokyo 194-8543
- ⁷⁵Soongsil University, Seoul 06978
- ⁷⁶Sungkyunkwan University, Suwon 16419
- ⁷⁷School of Physics, University of Sydney, New South Wales 2006
- ⁷⁸Department of Physics, Faculty of Science, University of Tabuk, Tabuk 71451
- ⁷⁹Tata Institute of Fundamental Research, Mumbai 400005
- ⁸⁰Department of Physics, Technische Universität München, 85748 Garching
- ⁸¹Toho University, Funabashi 274-8510
- ⁸²Department of Physics, Tohoku University, Sendai 980-8578
- ⁸³Earthquake Research Institute, University of Tokyo, Tokyo 113-0032
- ⁸⁴Department of Physics, University of Tokyo, Tokyo 113-0033
- ⁸⁵Tokyo Institute of Technology, Tokyo 152-8550
- ⁸⁶Virginia Polytechnic Institute and State University, Blacksburg, Virginia 24061
- ⁸⁷Wayne State University, Detroit, Michigan 48202
- ⁸⁸Yonsei University, Seoul 03722
- ⁸⁹Deutsches Elektronen-Synchrotron, 22607 Hamburg
- (Dated: January 6, 2022)

The measurement of two-particle angular correlation functions in high-multiplicity e^+e^- collisions at $\sqrt{s} = 10.52$ GeV is reported. In this study, the 89.5 fb^{-1} of hadronic e^+e^- annihilation data collected by the Belle detector at KEKB are used. Two-particle angular correlation functions are measured in the full relative azimuthal angle ($\Delta\phi$) and three units of pseudorapidity ($\Delta\eta$), defined by either the electron beam axis or the event-shape thrust axis, and are studied as a function of charged-particle multiplicity. The measurement in the thrust axis analysis, with mostly outgoing quark pairs determining the reference axis, is sensitive to the region of additional soft gluon emissions. No significant anisotropic collective behavior is observed with either coordinate analyses. Near-side jet correlations appear to be absent in the thrust axis analysis. The measurements are compared to predictions from various event generators and are expected to provide new constraints to the phenomenological models in the low-energy regime.

PACS numbers: 12.38.-t,12.38.Mh,25.75.-q

Two-particle angular correlations have been extensively studied in search of quark-gluon plasma (QGP) formation and its properties in nucleus-nucleus collisions [1–4] over the last several decades. In such collisions, a ridge-like structure of the correlation function, residing in a particular phase space where particle pairs have large differences in pseudorapidity but small differences in azimuthal angle, is observed. This signal in relativistic heavy ion collisions is interpreted as the macroscopic consequence of the hydrodynamical expansion of the perfect-fluid-like QGP state with the presence of initial density fluctuations [5–7]. The ridge-like signal was also observed in high charged-particle multiplicity events in proton-proton, proton-nucleus, deuteron-nucleus, and helium-nucleus collisions [8–16]. Recently, data on ultra-peripheral PbPb photonuclear collisions [17] also resulted in significant second- and third-order flow coefficients, which is an approach to quantify the two-particle azimuthal anisotropy with Fourier harmonics. Essentially, the ridge-like signal is reported in all collision systems involving at least one hadron. However, the physical origin of azimuthal anisotropies in these smaller collision systems is not yet fully understood [18, 19]. In hadron-hadron collisions, the complexity introduced by the initial state cannot be easily factored out. A large number of theoretical models based on different underlying mechanisms such as partonic initial-state correlations [20], final-state interactions [21, 22], and hydrodynamic medium expansion [23] have been proposed to explain the observed ridge-like signal in these small systems.

To break down the question, high charged-particle multiplicity events produced in the even smaller electron-ion and electron-positron collision systems are proposed to provide accessibility to understanding the cause of this special collective behavior [24]. As an example, a color dipole configuration (two color strings aligned in parallel with a gap in between) in the e^+e^- collision system can exhibit anisotropy in the initial parton geometry and generate ridge-like correlations. Recently, experimental studies have been extended to such smaller collision systems, e.g., electron-proton [25] and electron-positron (e^+e^-) [26] collisions. No significant ridge-like signal was observed in these measurements. These results

have stimulated discussions on the ways to search for and understand possible collectivity signatures in e^+e^- [27–29] and electron-ion collisions [30, 31]. However, the data samples used for the search in the e^+e^- ALEPH archived data [26] is small, which motivates the examination of a high-statistics data to study the highest multiplicity tail at Belle.

Taking advantage of the clean environment in e^+e^- collisions and high-statistics data collected with the Belle detector at KEKB [32], the analysis is performed for the first time at a center-of-mass energy of $\sqrt{s} = 10.52$ GeV, which is 60 MeV lower than the $\Upsilon(4S)$ resonance. Overall, a data sample of 89.5 fb^{-1} is utilized in this analysis, which is the full dataset of collisions at $\sqrt{s} = 10.52$ GeV. This analysis closely follows the previous analysis procedure with ALEPH archived data [26]. Although the average event multiplicity is lower than the ALEPH data, the two-particle correlation analysis is performed on the largest off-resonance Belle dataset, whose results can solidify previous findings. The Belle hadronic-event dataset is about four times larger than that with ALEPH archived data, enabling the collectivity search to move forward from a scan amongst the 0.5% highest multiplicity events of the total distribution to that of 0.02% percentile. Moreover, the measurement of the two-particle correlation function in the low-energy regime can provide additional inputs to the phenomenological fragmentation models.

The Belle detector is a large-solid-angle magnetic spectrometer that consists of a silicon vertex detector, a 50-layer central drift chamber, an array of aerogel threshold Cherenkov counters, a barrel-like arrangement of time-of-flight scintillation counters, and an electromagnetic calorimeter (ECL) comprising CsI(Tl) crystals located inside a superconducting solenoid coil that provides a 1.5 T magnetic field. An iron flux-return located outside of the coil is instrumented to detect K_L^0 mesons and muons. The detector is described in detail elsewhere [33].

The hadronic-event selection [34], including requirements on event multiplicity and energy sum in the ECL, is adopted to suppress contamination from two-photon, radiative Bhabha, and other QED events. Particles used in the calculation of the correlation functions are pri-

mary charged tracks, defined as prompt tracks or decay products of intermediate particles with proper lifetime $\tau < 1$ cm/ c . The corresponding selection on experimental data is tracks produced from the interaction point (including from short-lifetime particle decays) and tracks from long-lifetime particle decays with $V_r < 1$ cm, where V_r is the distance in the transverse plane of the decay vertex from the interaction point. The latter can intersect with other track on a common space-point and has dihadron invariant mass consistent with the mass of a K_S^0 (0.480-0.516 GeV/ c^2) or $\Lambda^0/\bar{\Lambda}^0$ (1.111-1.121 GeV/ c^2) candidate; otherwise, the track is deemed as a prompt track and accepted in the primary particle selection. Charged tracks are required to be within the detector acceptance, i.e., with polar angles ranging from 17° - 150° ($+z$ is defined opposite to the e^+ beam), and have transverse momenta in the center-of-mass frame greater than 0.2 GeV/ c . Impact parameter requirements are adopted to select charged tracks within ± 2 cm with respect to the interaction point in the transverse plane, and ± 5 cm along the z direction. For a pair of neighboring low-momentum tracks with the absolute value of cosine opening angle greater than 0.95 and transverse momenta below 0.4 GeV/ c , the one with less momentum is deemed as a duplicated track and is hence removed. Tracks from photon conversion candidates are vetoed, with the latter selected with the invariant mass less than 0.25 GeV/ c^2 and the decay-vertex radius greater than 1.5 cm.

To eliminate the effects of the nonuniform detection efficiency and misreconstruction bias, efficiency correction factors are derived by the Belle Monte Carlo (MC) sample. The Belle MC is simulated based on EVTGEN [35] and PYTHIA6 [36], where hadronic $q\bar{q}$ ($q = u, d, s, c$) fragmentation as well as low-multiplicity $e^+e^- \rightarrow \tau^+\tau^-$ and two-photon processes are taken into account. The detector response is simulated with GEANT3 [37]. The MC sample is further reweighted to match event multiplicity and thrust distributions of the data in order to correct for the imperfection in MC simulation. In order to study the multiplicity dependence of the correlation function, the events are binned into multiplicity classes using the reconstructed track multiplicity, denoted $N_{\text{trk}}^{\text{rec}}$, by counting tracks after all selections. For low-multiplicity events with $N_{\text{trk}}^{\text{rec}} < 12$, only a sample size of 11.5 fb^{-1} is used. The multiplicity classes used in this study, their corresponding fraction of data, and the mapping of average reconstructed multiplicities $\langle N_{\text{trk}}^{\text{rec}} \rangle$ to average multiplicities after efficiency correction $\langle N_{\text{trk}}^{\text{corr}} \rangle$ are listed in Table I.

The Belle experiment is operated with the KEKB asymmetric energy collider, colliding the 8 GeV electron beam and the 3.5 GeV positron beam. We boost events to their center-of-mass frame to perform the angular correlation analysis. Following a procedure similar to what has already been established in Ref. [10], the two-particle

TABLE I: Average multiplicities and corrected multiplicities of different $N_{\text{trk}}^{\text{rec}}$ intervals.

$N_{\text{trk}}^{\text{rec}}$ range	Fraction of data (%)	$\langle N_{\text{trk}}^{\text{rec}} \rangle$	$\langle N_{\text{trk}}^{\text{corr}} \rangle$
[6, 10)	44.33	6.98	7.05
[10, 12)	2.65	10.26	10.12
[12, 14)	0.29	12.20	11.90
[14, ∞)	0.02	14.22	14.24

correlation function observable is defined as

$$\frac{1}{N_{\text{trk}}^{\text{corr}}} \frac{d^2 N^{\text{pair}}}{d\Delta\eta d\Delta\phi} = B(0, 0) \times \frac{S(\Delta\eta, \Delta\phi)}{B(\Delta\eta, \Delta\phi)}. \quad (1)$$

The correlation function is expressed in terms of the particle pair's angular difference $\Delta\eta = \pm(\eta_i - \eta_j)$ and $\Delta\phi = \pm(\phi_i - \phi_j)$, where i, j label the track pair's indices. The calculation is based on an assumption of correlations being symmetric about the origin $(\Delta\eta, \Delta\phi) = (0, 0)$; hence, four entries are counted for a given pair. The per-charged-particle associated track-pair yield is denoted as N^{pair} , and is reweighted by efficiency correction factors of both particles. The signal correlation $S(\Delta\eta, \Delta\phi)$ and the background correlation $B(\Delta\eta, \Delta\phi)$ can be explicitly written out as

$$\begin{aligned} S(\Delta\eta, \Delta\phi) &= \frac{1}{N_{\text{trk}}^{\text{corr}}} \frac{d^2 N^{\text{same}}}{d\Delta\eta d\Delta\phi}, \\ B(\Delta\eta, \Delta\phi) &= \frac{1}{N_{\text{trk}}^{\text{corr}}} \frac{d^2 N^{\text{mix}}}{d\Delta\eta d\Delta\phi}, \end{aligned} \quad (2)$$

where N^{same} (N^{mix}) counts the number of track-pairs formed by matching the i -th charged particle of a given event with the j -th particle in the same event ("mixed event" [8]). A mixed event in this work is a combination of tracks from three random events and is normalized by a factor of $1/3$. Three random events are chosen such that their $N_{\text{trk}}^{\text{rec}}$'s are the same as that of the event they match to. The $B(0, 0)$ factor is incorporated in the calculation of the correlation function, serving as the normalization of the artificially constructed $B(\Delta\eta, \Delta\phi)$. This factor is obtained by extrapolating the function value to the origin of $B(\Delta\eta, \Delta\phi)$. An additional correction on the correlation function is applied to deal with the effects introduced by using finite-bin histogramming to approximate the density function. The bin-size effect is modeled by a second-order polynomial and the magnitude of the correlation function is calibrated. To unfold back to the truth level, final correlations are corrected with the bin-by-bin method [38], accounting for residual reconstruction effects after efficiency corrections.

The two-particle correlation function is explored in two coordinate systems: beam and thrust axis coordinates in

the e^+e^- center-of-mass frame. The former is the same as that presented in most of the two-particle correlation studies, while in the latter, initiated by Ref. [26], the event thrust axis [39] is used as the reference axis, with missing momentum of the event included. The construction of mixed events in the thrust axis analysis is identical to that in the beam axis analysis, requiring the multiplicity matching only. In the thrust axis coordinate analysis, the kinematics (p_T, η, ϕ) of a mixed event are calculated with respect to the thrust axis of its matched physical event. To adjust the kinematic distribution of the mixed event to physical kinematic (p_T, η, ϕ) spectra, a reweighting correction is adopted.

In the e^+e^- annihilation process, when the interacting system is located in between or along the color string connecting the $q\bar{q}$ pair, measuring with a coordinate system defined by the event thrust axis provides a more direct picture. From the viewpoint of relativistic fluid dynamics [7], conventional beam-axis measurements are sensitive to features within the plane transverse to the collision axis, probing any anisotropic behavior of the QCD medium, which are widely studied as the phenomena of elliptic or triangular flow [6, 40, 41]. The insensitive region of the two-particle correlation function in the beam axis analysis is at the beam pipe, where a particle pair with a large pseudorapidity difference is excluded from the finite $\Delta\eta$ region of interest (e.g., $|\Delta\eta| \leq 3.0$ in this analysis). In addition, the on-axis track-pair correlation is too deformed to form an obvious correlation structure, since the ϕ coordinate is ill-represented near both poles of the spherical coordinate. Correspondingly, the insensitivity of the thrust-axis correlation function is at its reference thrust axis which quark-initiated dijets are close to; however, they are sensitive in the mid-rapidity region, where additional soft gluons emit apart from the leading quark-antiquark dijet-like structure. The sensitivity to the finer structure allows one to check in details if there are special correlations among the color activity in the small system.

In Fig. 1, correlation functions with multiplicity $N_{\text{trk}}^{\text{rec}} \geq 12$ are shown for both beam and thrust axis coordinates. In the beam axis coordinate view, the peak near the origin $(\Delta\eta, \Delta\phi) = (0, 0)$ has contributions from pairs originating in the same jet, while the structure at $\Delta\phi \approx \pi$ is from back-to-back correlations. These features reflect the two-particle correlation of dijet-like $q\bar{q}$ events, which mainly contribute in e^+e^- collisions. In contrast, for the thrust axis coordinates, the dominant structure is the hill-like bump near $(\Delta\eta, \Delta\phi) \approx (0, \pi)$, while a sizeable near-side correlation is lacking. The decrease of the near-side-peak correlation is because that leading two jets are brought to insensitive regions around poles of the reference thrust axis. As a result of balance for the event thrust calculation, track pairs amongst on-axis jets tend to yield larger $\Delta\phi$ angular differences. Compared to collisions at high center-of-mass energies, jets are composed

of fewer constituents and have broader shapes at the low energy regime. This makes it hard to form a significant near-side-peak correlation. We calculated the magnitude of the near-side-peak correlation with respect to different collision energies with SHERPA 2.2.5 [42] simulation of $e^+e^- \rightarrow$ hadrons at the leading order, and found results suggesting a significant correspondence.

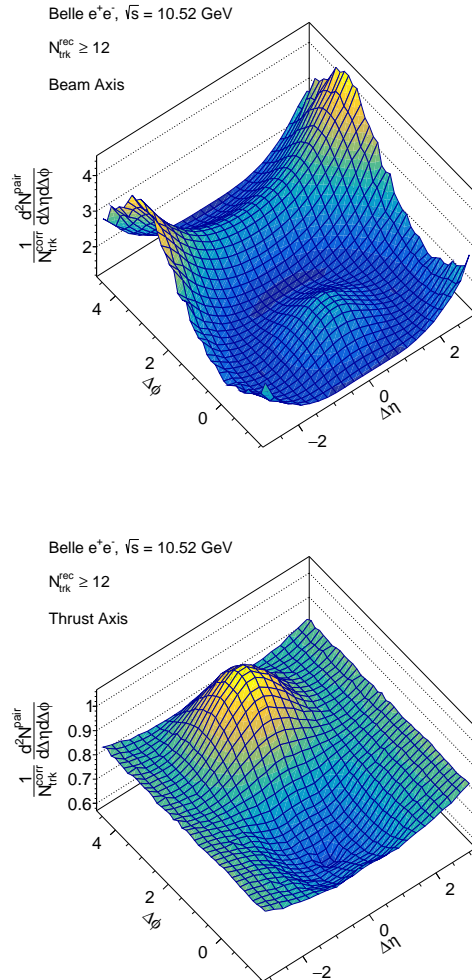


FIG. 1: Two-particle correlation functions for beam (top) and thrust (bottom) axis analyses with the multiplicity $N_{\text{trk}}^{\text{rec}} \geq 12$.

Evidence for the ridge signal can be best examined in the azimuthal differential yield $Y(\Delta\phi)$ by averaging the correlation function over the long-range region with $1.5 \leq |\Delta\eta| < 3.0$. A “zero yield at minimum” (ZYAM) method [43] is further implemented to separate any enhanced near-side correlation around $\Delta\phi = 0$ distinct from a constant correlation. The constant contribution along $\Delta\phi$, denoted as C_{ZYAM} , is estimated by the minimum of the fit with a third-order Fourier series to the data points. A fit with a third-order polynomial plus a cosine term, and with a fourth-order polynomial are also checked to

estimate C_{ZYAM} in parallel.

The systematic uncertainties due to the selection and correction operations are calculated with respect to long-range $Y(\Delta\phi)$. Hadronic-event selection is examined by tightening the energy sum requirement in the ECL from $E_{\text{sum}} > 0.18\sqrt{s}$ to $0.23\sqrt{s}$. The primary-particle selection systematic is estimated by making variations of the proper lifetime requirement $\tau < 1$ cm/c and the vertex $V_r < 1$ cm. In general, results from both variations differ by less than 1% (or by 1-6% for the high-multiplicity bin). A 0.35% uncertainty is quoted for the tracking reconstruction efficiency, which is evaluated by comparing partially and fully reconstructed $D^* \rightarrow \pi_{\text{slow}} D^0 (\rightarrow \pi^+ \pi^- K_S^0 (\rightarrow \pi^+ \pi^-))$ decays [44]. In the beam axis analysis, the systematic uncertainties are mainly from the primary-particle selection and the tracking efficiency, which are in general on the order of 0.3%–0.4%, while the primary-particle selection increases to a 6.3% uncertainty for high-multiplicity events with $N_{\text{trk}}^{\text{rec}} \geq 14$. For high-multiplicity event classes in the thrust axis analysis, dominant sources of systematic uncertainties are due to the event selection ($< 2\%$) and the primary-particle selection ($< 4\%$), where the estimation of uncertainties suffers from the need for large statistics to derive a precise reweighting factor for the efficiency correction and for the mixed events. On the other hand, for low-multiplicity classes, the dominant source of uncertainty is due to tracking. Other uncertainties originate from MC reweighting, the $B(0,0)$ factor, mixed events reweighting, scaling corrections due to bin effects and residual bin effects, all of which are checked to be small in different multiplicity bins (of order $\mathcal{O}(10^{-4})$), with the largest one contributing up to 0.3% uncertainty.

Figure 2 shows the measurement of long-range $Y(\Delta\phi)$ after performing the ZYAM method, along with a comparison of predictions from Belle MC, HERWIG 7.2.2 [45], and SHERPA 2.2.5 [42] event generators. The region with small azimuthal angle difference ($\Delta\phi \approx 0$) is where possible ridge signals would be visible as a nonzero value. In the beam axis coordinates, all generators are consistent with data in the near-side ridge region, but HERWIG and SHERPA undershoot the data in the away-side region. In the thrust axis analysis, the Belle simulation, with specific tunes adapted to Belle data, gives again a better description of these correlation data. A larger discrepancy from the data is seen in the HERWIG simulation. An excess of correlations is showing up in the near-side ridge-prone region and there is also an overshoot in the away-side region.

The significance of any ridge signal can be quantified by integrating over $Y(\Delta\phi)$ from $\Delta\phi = 0$ to where the ZYAM fit minimum occurs. Ridge yields smaller than an order of 10^{-10} are measured. Since there is no obvious ridge-like structure in either the beam or thrust axis analysis, a bootstrap procedure [46] is implemented and the confidence limit of the integrated ridge yield is reported. In the bootstrap procedure, each azimuthal differential

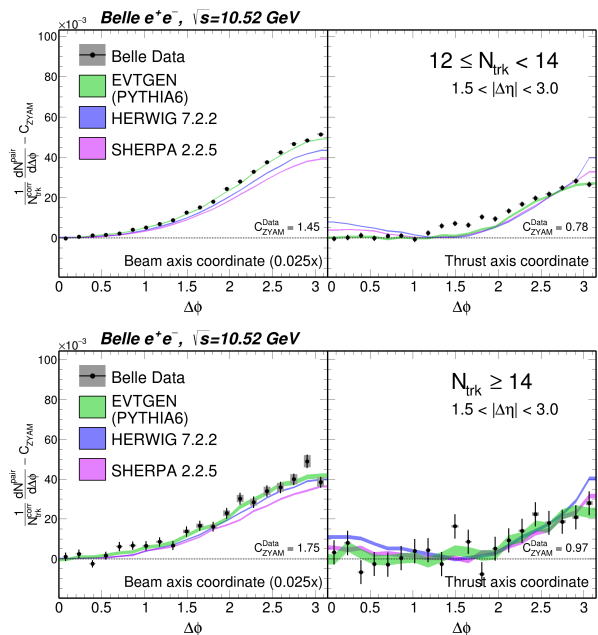


FIG. 2: Comparison of ZYAM-subtracted $Y(\Delta\phi)$ in the range $1.5 < |\Delta\eta| < 3.0$ for the multiplicity $12 \leq N_{\text{trk}}^{\text{rec}} < 14$ (top) and $N_{\text{trk}}^{\text{rec}} \geq 14$ (bottom), where subtracted constants of data C_{ZYAM}^{Data} are quoted. In each panel, results for beam (left) and thrust (right) axis analyses are displayed. The colored bands show simulation predictions from Belle MC (green), HERWIG (blue), and SHERPA (violet). The error bars on the data represent the statistical uncertainties, and the gray boxes are systematic uncertainties. For visual purposes, the minimal statistical uncertainty of the MC colored bands is set to be 3×10^{-4} , and beam-axis ZYAM-subtracted yields are scaled by a factor of 0.025.

yield distribution is varied according to their statistical and systematic uncertainties, and the yield distribution is sampled 2×10^6 times. For the ZYAM subtraction, three fit templates (a third-order Fourier series, a third-order polynomial plus a cosine term, and a fourth-order polynomial) are attempted, of which the most conservative confidence limit is quoted. In Fig. 3, the 95% confidence level upper limits as a function of $\langle N_{\text{trk}}^{\text{corr}} \rangle$ are reported. For the ridge yield upper limit less than 10^{-7} , we report the confidence levels of the ridge signal exclusion, instead.

In summary, the first measurement of two-particle correlations of hadrons in beam and thrust axis coordinate systems, performed using e^+e^- collision data at $\sqrt{s} = 10.52$ GeV from Belle is reported. A strong exclusion of ridge yield in the beam axis coordinate analysis is set. In the thrust axis coordinate analysis, there is no significant near-side-peak correlation, different from what was observed in hadronic collisions or high-energy e^+e^- collisions. A 95-97% confidence level upper limit or a 5σ exclusion is set versus $\langle N_{\text{trk}}^{\text{corr}} \rangle$ for the absence of any ridge yield in our measurement. Though there is no hint

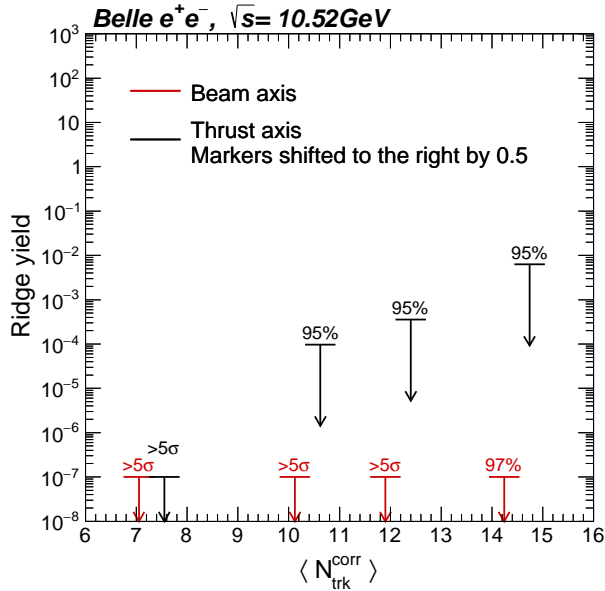


FIG. 3: Upper limits of the ridge yield as a function of $\langle N_{\text{trk}}^{\text{corr}} \rangle$ in beam axis (red) and thrust axis (black) coordinate frames. Thrust axis limits are shifted to the right by 0.5 for presentation purposes. The label “ $> 5\sigma$ ” indicates the 5σ confidence level upper limit.

of collectivity signals in the low-energy e^+e^- collision system, the measurement can be provided as a reference for tunes of fragmentation models in the soft QCD scale. Belle MC samples based on EVTGEN (with a PYTHIA6 interface for $e^+e^- \rightarrow q\bar{q}$ generation), along with HERWIG and SHERPA event generators are examined. Similar to the conclusion from the previous analysis with ALEPH archived data [26], the results in this study are found to be better described by PYTHIA6 than SHERPA or HERWIG.

We thank the KEKB group for the excellent operation of the accelerator; the KEK cryogenics group for the efficient operation of the solenoid; and the KEK computer group, and the Pacific Northwest National Laboratory (PNNL) Environmental Molecular Sciences Laboratory (EMSL) computing group for strong computing support; and the National Institute of Informatics, and Science Information Network 5 (SINET5) for valuable network support. We acknowledge support from the Ministry of Education, Culture, Sports, Science, and Technology (MEXT) of Japan, the Japan Society for the Promotion of Science (JSPS), and the Tau-Lepton Physics Research Center of Nagoya University; the Australian Research Council including grants DP180102629, DP170102389, DP170102204, DP150103061, FT130100303; Austrian Federal Ministry of Education, Science and Research (FWF) and FWF Austrian Science Fund No. P 31361-N36; the

National Natural Science Foundation of China under Contracts No. 11435013, No. 11475187, No. 11521505, No. 11575017, No. 11675166, No. 11705209; Key Research Program of Frontier Sciences, Chinese Academy of Sciences (CAS), Grant No. QYZDJ-SSW-SLH011; the CAS Center for Excellence in Particle Physics (CCEPP); the Shanghai Science and Technology Committee (STCSM) under Grant No. 19ZR1403000; the Ministry of Education, Youth and Sports of the Czech Republic under Contract No. LTT17020; Horizon 2020 ERC Advanced Grant No. 884719 and ERC Starting Grant No. 947006 “InterLeptons” (European Union); the Carl Zeiss Foundation, the Deutsche Forschungsgemeinschaft, the Excellence Cluster Universe, and the VolkswagenStiftung; the Department of Atomic Energy (Project Identification No. RTI 4002) and the Department of Science and Technology of India; the Istituto Nazionale di Fisica Nucleare of Italy; National Research Foundation (NRF) of Korea Grant Nos. 2016R1D1A1B-01010135, 2016R1D1A1B02012900, 2018R1A2B3003643, 2018R1A6A1A06024970, 2019K1A3A7A09033840, 2019R1I1A3A01058933, 2021R1A6A1A03043957, 2021R1F1A1060423, 2021R1F1A1064008; Radiation Science Research Institute, Foreign Large-size Research Facility Application Supporting project, the Global Science Experimental Data Hub Center of the Korea Institute of Science and Technology Information and KREONET/GLORIAD; the Polish Ministry of Science and Higher Education and the National Science Center; the Ministry of Science and Higher Education of the Russian Federation, Agreement 14.W03.31.0026, and the HSE University Basic Research Program, Moscow; University of Tabuk research grants S-1440-0321, S-0256-1438, and S-0280-1439 (Saudi Arabia); the Slovenian Research Agency Grant Nos. J1-9124 and P1-0135; Ikerbasque, Basque Foundation for Science, Spain; the Swiss National Science Foundation; the Ministry of Education and the Ministry of Science and Technology of Taiwan; and the United States Department of Energy and the National Science Foundation.

* now at Massachusetts Institute of Technology

† also at University of Petroleum and Energy Studies, Dehradun 248007

- [1] I. Arsene et al. (BRAHMS Collaboration), Nucl. Phys. A **757**, 1 (2005), arXiv:nucl-ex/0410020.
- [2] B. Back et al. (PHOBOS Collaboration), Nucl. Phys. A **757**, 28 (2005), arXiv:nucl-ex/0410022.
- [3] J. Adams et al. (STAR Collaboration), Nucl. Phys. A **757**, 102 (2005), arXiv:nucl-ex/0501009.
- [4] K. Adcox et al. (PHENIX Collaboration), Nucl. Phys. A **757**, 184 (2005), arXiv:nucl-ex/0410003.
- [5] J.-Y. Ollitrault, Phys. Rev. D **46**, 229 (1992).
- [6] B. Alver and G. Roland, Phys. Rev. C **81**, 054905 (2010), [Erratum: Phys.Rev.C **82**, 039903 (2010)],

- arXiv:1003.0194.
- [7] U. Heinz and R. Snellings, *Ann. Rev. Nucl. Part. Sci.* **63**, 123 (2013), arXiv:1301.2826.
- [8] V. Khachatryan et al. (CMS Collaboration), *JHEP* **09**, 091 (2010), arXiv:1009.4122.
- [9] G. Aad et al. (ATLAS Collaboration), *Phys. Rev. Lett.* **116**, 172301 (2016), arXiv:1509.04776.
- [10] S. Chatrchyan et al. (CMS Collaboration), *Phys. Lett. B* **718**, 795 (2013), arXiv:1210.5482.
- [11] B. Abelev et al. (ALICE Collaboration), *Phys. Lett. B* **719**, 29 (2013), arXiv:1212.2001.
- [12] G. Aad et al. (ATLAS Collaboration), *Phys. Rev. Lett.* **110**, 182302 (2013), arXiv:1212.5198.
- [13] A. Adare et al. (PHENIX Collaboration), *Phys. Rev. Lett.* **111**, 212301 (2013), arXiv:1303.1794.
- [14] S. Chatrchyan et al. (CMS Collaboration), *Eur. Phys. J. C* **72**, 2012 (2012), arXiv:1201.3158.
- [15] R. Aaij et al. (LHCb Collaboration), *Phys. Lett. B* **762**, 473 (2016), arXiv:1512.00439.
- [16] J. Adam et al. (STAR Collaboration), *Phys. Rev. Lett.* **122**, 172301 (2019), arXiv:1901.08155.
- [17] G. Aad et al. (ATLAS Collaboration), *Phys. Rev. C* **104**, 014903 (2021), arXiv:2101.10771.
- [18] K. Dusling, W. Li and B. Schenke, *Int. J. Mod. Phys. E* **25**, 1630002 (2016), arXiv:1509.07939.
- [19] J. L. Nagle and W. A. Zajc, *Ann. Rev. Nucl. Part. Sci.* **68**, 211 (2018), arXiv:1801.03477.
- [20] K. Dusling and R. Venugopalan, *Phys. Rev. D* **87**, 094034 (2013), arXiv:1302.7018.
- [21] L. He et al., *Phys. Lett. B* **753**, 506 (2016), arXiv:1502.05572.
- [22] C. Bierlich, G. Gustafson and L. Lönnblad, *Phys. Lett. B* **779**, 58 (2018), arXiv:1710.09725.
- [23] P. Bozek, *Phys. Rev. C* **85**, 014911 (2012), arXiv:1112.0915.
- [24] J. L. Nagle et al., *Phys. Rev. C* **97**, 024909 (2018), arXiv:1707.02307.
- [25] I. Abt et al. (ZEUS Collaboration), *JHEP* **04**, 070 (2020), arXiv:1912.07431.
- [26] A. Badea et al., *Phys. Rev. Lett.* **123**, 212002 (2019), arXiv:1906.00489.
- [27] C. Bierlich, S. Chakraborty, G. Gustafson and L. Lönnblad, *JHEP* **03**, 270 (2021), arXiv:2010.07595.
- [28] P. Castorina, D. Lanteri and H. Satz, *Eur. Phys. J. A* **57**, 111 (2021), arXiv:2011.06966.
- [29] A. Baty, P. Gardner and W. Li (2021), arXiv:2104.11735.
- [30] Y. Shi, L. Wang, S.-Y. Wei, B.-W. Xiao and L. Zheng, *Phys. Rev. D* **103**, 054017 (2021), arXiv:2008.03569.
- [31] P. Agostini et al. (LHeC, FCC-he Study Group Collaboration) (2020), arXiv:2007.14491.
- [32] S. Kurokawa and E. Kikutani, *Nucl. Instrum. Methods Phys. Res. Sect. A* **499**, 1 (2003), and other papers included in this Volume; T. Abe *et al.*, *Prog. Theor. Exp. Phys.* **2013**, 03A001 (2013) and references therein.
- [33] A. Abashian *et al.* (Belle Collaboration), *Nucl. Instrum. Methods Phys. Res. Sect. A* **479**, 117 (2002); also see Section 2 in J. Brodzicka *et al.*, *Prog. Theor. Exp. Phys.* **2012**, 04D001 (2012).
- [34] K. Abe et al. (Belle Collaboration), *Phys. Rev. D* **64**, 072001 (2001), arXiv:hep-ex/0103041.
- [35] A. Ryd et al. (2005), EVTGEN-V00-11-07.
- [36] T. Sjöstrand et al., *Comput. Phys. Commun.* **135**, 238 (2001), arXiv:hep-ph/0010017.
- [37] R. Brun et al., CERN Report DD/EE/84-1 (1984).
- [38] G. Choudalakis (ATLAS Collaboration), in *PHYSTAT 2011* (CERN, Geneva, 2011), arXiv:1104.2962.
- [39] E. Farhi, *Phys. Rev. Lett.* **39**, 1587 (1977).
- [40] T. A. Trainor, *Phys. Rev. C* **81**, 014905 (2010).
- [41] K. Aamodt et al. (ALICE Collaboration), *Phys. Rev. Lett.* **105**, 252302 (2010).
- [42] E. Bothmann et al. (Sherpa Collaboration), *SciPost Phys.* **7**, 034 (2019), arXiv:1905.09127.
- [43] N. N. Ajitanand et al., *Phys. Rev. C* **72**, 011902 (2005), arXiv:nucl-ex/0501025.
- [44] Ed. A.J. Bevan, B. Golob, Th. Mannel, S. Prell, and B.D. Yabsley, *Eur. Phys. J. C* **74**, 3026 (2014), arXiv:1406.6311.
- [45] J. Bellm et al., *Eur. Phys. J. C* **76**, 196 (2016), arXiv:1512.01178.
- [46] B. Efron, *Ann. Statist.* **7**, 1 (1979).